*Proceedings of the 6th International Conference on Energy Harvesting, Storage, and Transfer (EHST'22)*
*Niagara Falls, Canada – June 08-10, 2022*
*Paper No. 142 (The number assigned by the OpenConf System)*
*DOI: 10.11159/ehst22.142*

# Theoretical and Computational Models of the Performance of a Cylindrical Thermo-Chemical Battery During Charging and Operational Modes

**Seyyed Ali Hedayat Mofidi[1], Kent S. Udell[1]**
[1]Mechanical Engineering Department, University of Utah
1495 E 100S, 1550 MEK, Salt Lake City, Utah, USA
Ali.Hedayat@Utah.edu; Kent.Udell@utah.edu

***Abstract*** – Thermo-Chemical batteries are a versatile way to store thermal energy. Once charged, thermo-chemical batteries can provide any combination of refrigeration, space cooling, heating and food processing. Due to favourable temperature ranges, material abundance and sustainable sources of necessary elements, and their high energy storage density, $MgCl_2/NH_3$ thermochemical batteries are of particular interest.

In this paper, the performance of $MgCl_2/NH_3$ thermochemical batteries is quantified through a series of numerical and theoretical studies of a representative geometry. The models consider a cylinder either cooled from the outside surface or a cooling tube located along its axis. It is found that cooling from a central tube provides best potential for applications of constant cooling rate for duration of discharge. The thermal performance of the various ratios of inner tube radius to cylinder wall radius are presented. In our previous studies [1], [2], various 2-D cylindrical cooling configurations were numerically simulated to determine the parameters that improve the performance of thermochemical thermal energy storage. In particular, a $MgCl_2.2NH_3$ salt's ability to absorb $NH_3$ at a relatively uniform rate was evaluated for a cylinder heated both internally and externally. Simulations exhibited behaviour typical of shrinking core responses to heating and cooling, thus motivating theoretical models are to generalize the simulation results, and to extend the analysis to the heating or recharge mode.

The models consider a cylinder either heated or cooled from the outside surface or from a tube located along its axis. Equations are developed to track the advance of the reaction front as controlled by heat transfer. Explicit relations relate absorption or desorption mass fluxes, operation times, and extent of reactions to the location of the reaction front for the two geometries given forcing temperature differences and salt complex thermal properties. The analytical model is compared with simulations for $MgCl_2.2NH_3$ in the cooling mode, with very good agreement between computed mass flow rates, degree of reaction and location of the ammonia absorption fronts. The extension of the model to other complexes and generalization of the model to the recharge mode provides a convenient tool to estimate design parameters for applications representing differing storage timescales, dimensions, salt properties, driving temperature differences, and geometries.

***Keywords*****:** Magnesium Chloride, Ammonia, Thermal Energy Storage, Solid-gas Reactor

## 1. Introduction

As outlined in previous research studies [1]–[7], the storage of energy in a thermochemical battery comprised of a $MgCl_2/NH_3$ pair is of broad interest because the stored heat from a source with a temperature near or above 250°C can be returned to provide refrigeration (T < 0°C), air cooling and heating, and food preparation heat (T > 200°C). In such a thermochemical energy storage system at fully charged state, the ammonia is stored in a tank, ready to vaporize once exposed to the low equilibrium pressure of the salt at ambient temperatures. Thus, upon the opening of a valve separating the ammonia tank from the salt complex, the temperature of the salt complex increases to an equilibrium temperature determined by vapor pressure of the ammonia from the tank.

After this "start-up" period, the thermochemical battery performance will become limited by heat transfer in the salt matrix. This is exacerbated by the orders of magnitude drop in gas permeability as the salt becomes fully saturated with ammonia [2] restricting gas flows to locations where the salt is cooled. These elements lead to a design solution where the geometry of the salt and cooling method is chosen to minimize heat transfer resistance between the cooling fluid and the reaction zone where the heat is being generated by the vapor absorption. Cylindrical geometries, with uniform cooling of the exterior wall or by a tube on the axis carrying cooling fluids, have been found to be good choices for optimal design as long as sufficient axial gas permeabilities exist [1], [2], [8].

Numerical solutions have shown wave-like behaviour of the reaction front [1], [2], [9]–[11]. Figure 1 shows the profiles of reaction extent at various times for a case where the heat transfer was limited by the fluid-wall heat transfer coefficient on the axis (left boundary) of the domain. As observed from the advancement of the reaction front, and the computed temperatures on either side of the front, the reaction wave progresses at a rate determined by the heat transfer away from the front. Thus, a simplified analytical solution can be developed to generalize the predicted performance of thermochemical batteries given the properties of the absorbent, the dimensions of the reactor, and the driving temperature difference.

Further, the recharge phase, where the desorption front moves in response to heating, can also be modelled in the same manner. In that application, the equilibrium temperature is set by the imposed ammonia vapor pressure, and the reactive complex is heated to a temperature above that equilibrium value on the outside or from an internal tube [1], [2]. For a 2-D condition where the desorbed ammonia flows through the matrix in an axial direction, one may assume insignificant radial velocities or axial temperature gradients. Thus, the energy transport equation reduces to radial conduction alone - the conditions modelled in this study.

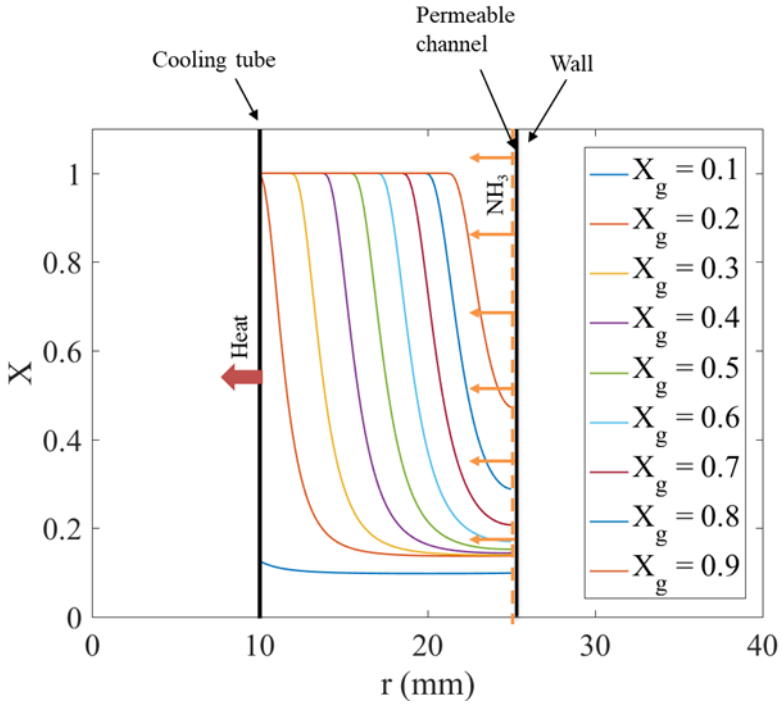


Figure 1 - Profiles of reaction progress (X) at milestones of global reaction progress ($X_g$).

## 2. Theoretical Models

In order to generalize the results of [1], the problem is cast as a moving reaction interface model with the time rate of change of the reaction zone radius is limited by the net heat transfer rate to the reaction interface. The pressure of the gas throughout the reactor is assumed constant at $P = P_{sup}$. This is achievable by the having a low-density reaction complex, or adding gas diffusion channels to the salt. It is further assumed that the sensible heat required to change the matrix temperature from the equilibrium value to the wall temperature is much less than the energy of absorption. Thus, the sensible energy of temperature transients is neglected. And lastly, the wall or tube temperature is assumed to remain constant during charging or discharging modes. Figure 2 shows the geometry of the reacting core models for the cases that the reactive complex is cooled from outer surface or an inner tube.

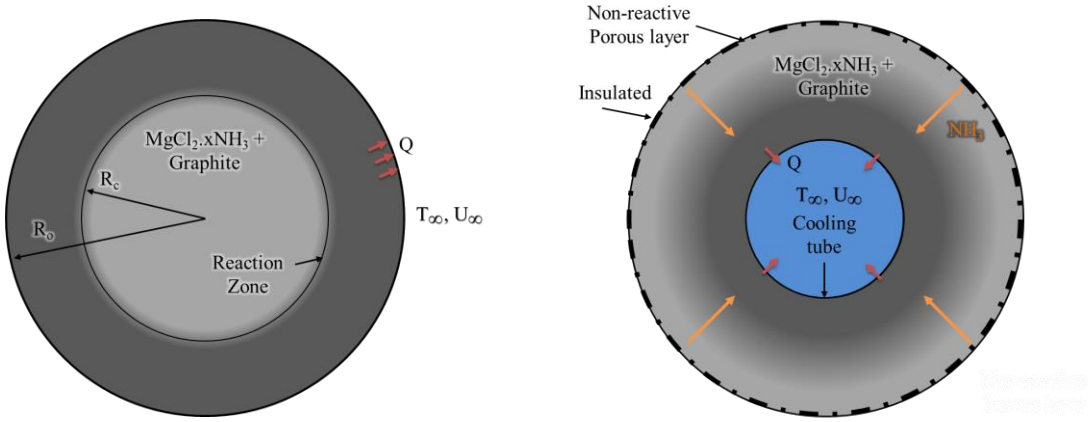


A) B)

Figure 2 - The geometry of the reacting core model for (A) geometries cooled from the outside and (B) cooled from an internal tube.

### 2.1. External Cooling or Heating

For a long cylinder heated or cooled from the outside boundaries, the reaction front will propagate inwards from the surface. The flow of heat is assumed to occur in the radial direction only and the reaction zone, as shown by [1], [2], is assumed to be infinitesimally small occurring at the radius $r_c$.

Neglecting the sensible heat loss or gain in either the fully saturated subcooled zone, or the completely desorbed matrix of the heated zone, the radial temperature distribution is that of the steady-state heat transfer in a cylindrical domain with the equilibrium temperature imposed at the reaction front and the wall temperature specified at the outer radius, $R_o$. Specifically, for cooling:

$$\frac{(T-T_s)}{(T_{eq}-T_s)} = \frac{\ln(R_o/r)}{\ln(R_o/r_c)} \tag{1}$$

And for heating:

$$\frac{(T-T_{eq})}{(T_s-T_{eq})} = 1 - \frac{\ln(R_o/r)}{\ln(R_o/r_c)} \tag{2}$$

The scaled temperature profiles of Eq. (1) and (2) are illustrated in Figure 3 for conceptual purposes. Three profiles are shown for different times with the reaction front location being different as it propagates away from the surface. For heating, the scaled surface temperature is 1 while the scaled interface temperature is 0. For cooling, the scaled surface temperature is 0 and the scaled equilibrium temperature is 1. For either of these cases, the heat transfer from the reaction interface to the surface per, unit length is:

$$\dot{Q} = \frac{2\pi\lambda(T_{eq}-T_s)}{\ln(R_o/r_c)} \tag{3}$$

The volumetric heat generation in the reaction zone is equal to

$$q = 4\bar{\rho}_{salt}\Delta H_r \tag{4}$$

$\Delta H_r$ in Eq. (4) is the enthalpy of the reaction per mole of ammonia gas absorbed in *kJ/kmole of gas*, $\bar{\rho}_{salt}$ is the molar density of salt, and a multiplier of 4 is required since one mole of salt absorbs 4 moles of ammonia gas. For the reaction front to move, this energy of reaction must be balanced by the heat transfer to (or from) the reaction front. Thus, the rate of the reaction front movement is directly related to the net energy conducted from (or to) the reaction front, or:

$$-4\bar{\rho}_{salt}\Delta H_r \times 2\pi r_c \times \frac{dr_c}{dt} = \frac{2\pi\lambda}{\ln(R_o/r_c)}\left(T_{eq} - T_\infty\right) \tag{5}$$

In Eq. (5), $r_c$ is the radius of the reaction zone, $R_o$ is the inner radius of the reactor tube, $T_\infty$ is the temperature at the surface of the reactive complex, and $\lambda$ is the effective thermal conductivity of the reactive complex.

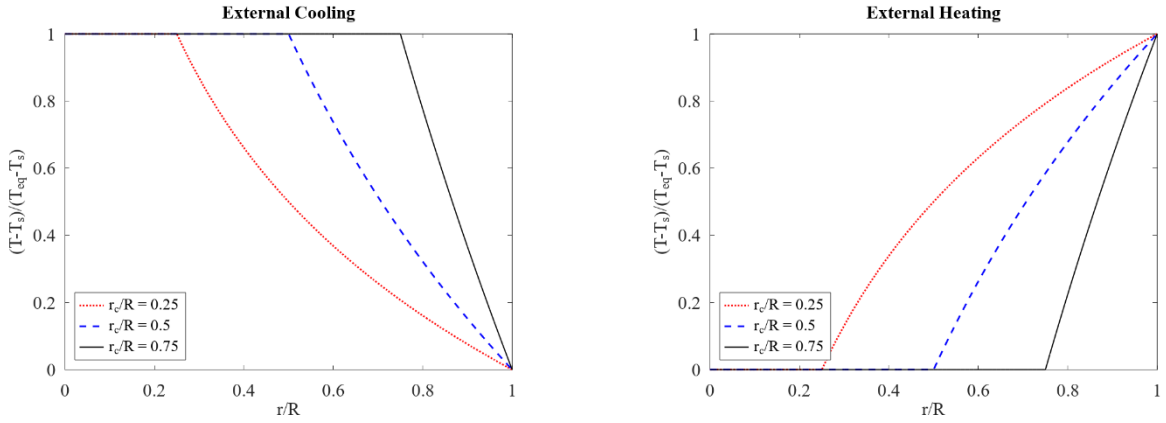


A) B)

Figure 3 - Scaled temperature fields for (A) External cooling, and (B) External heating

Equation (5) can be rewritten as:

$$r_c \ln\frac{r_c}{R_o} dr_c = \frac{\lambda}{\Delta H_r \times 4\bar{\rho}_{salt}}\left(T_{eq} - T_\infty\right)dt \tag{6}$$

Integrating both sides of Eq. (6) and applying the initial condition of $r_c = R_o$ at $t = 0$ gives:

$$\left(\frac{r^2}{2}(\ln r - \ln R_o) - \frac{r^2}{4}\right)_{R_o}^{r_c} = \frac{\lambda}{\Delta H_r \times 4\bar{\rho}_{salt}}\left(T_{eq} - T_\infty\right)t \tag{7}$$

The initial condition for the solution of Eq. (7) is set at the point that the reaction zone starts moving from the heat transfer boundary (roughly at $X_g = 0.2$), and not the start of the absorption or desorption processes. During the initial absorption or desorption, the reaction is volumetrically uniform until the compound reaches the equilibrium temperature that corresponds to the applied vapor pressure. Therefore, the initial condition on the global absorption process becomes:

$$X_g = 0.2 \quad \text{at } t = 0 \tag{8}$$

The relation between $X_g$ and the radius of the reaction zone ($r_c$) is shown in Eq. (8). In order to normalize $X_g$ to the range between $X_g = 0.2$ and $X_g = 1$, $X_{gs}$ is defined as scaled reaction progress:

$$X_{gs} = \frac{X_g - 0.2}{0.8} = 1 - \left(\frac{r_c}{R_o}\right)^2 \tag{9}$$

Equation (7) becomes:

$$\left[\frac{r_c^2}{2}\ln\frac{r_c}{R_o} - \frac{r_c^2}{4} - \left(\frac{R_o^2}{2}(\ln R_o - \ln R_o) - \frac{R_o^2}{4}\right)\right] = \frac{\lambda}{\Delta H_r \times 4\bar{\rho}_{salt}}\left(T_{eq} - T_\infty\right)t \tag{10}$$

After simplifying the terms and dividing both sides by $R_o^2$, Eq. (10) can be written in a dimensionless form:

$$\frac{1}{4}\left(\frac{r_c^2}{R_o^2}\ln\frac{r_c^2}{R_o^2} + \left(1 - \frac{r_c^2}{R_o^2}\right)\right) = \frac{\lambda}{\frac{\Delta H_r}{(T_{eq} - T_\infty)} \times 4\bar{\rho}_{salt}}\frac{t}{R_o^2} = Fo_r \tag{11}$$

The reaction Fourier number ($Fo_R$) is based on the reaction enthalpy divided by the driving temperature difference rather than the traditional material heat capacity used in the traditional definition. One can also show that the reaction Fourier number is the normal Fourier number multiplied by reaction Jakob number ($Ja_r = \bar{c_p}\left(T_{eq} - T_\infty\right)/\Delta H_r$). Solving Eq. (9) for the ratio $r_c/R_o$, and substituting it into Eq. (11), one can derive the following relationship for the reaction Fourier number and the global extent of the reaction.

$$\frac{1}{4}\left(\left(1 - X_{gs}\right)\ln\left(1 - X_{gs}\right) + X_{gs}\right) = Fo_R \tag{12}$$

The mass flow rate of ammonia for reactors with external cooling can be calculated from Eq. (4) directly:

$$\dot{m}_{NH_3} = 4\bar{\rho}_{salt} \times M_{NH_3} \times 2\pi r_c L \times \frac{dr_c}{dt} \tag{13}$$

Since

$$4\bar{\rho}_{salt} \times 2\pi r_c L \times \frac{dr_c}{dt} = \frac{2\pi L\lambda\left(T_{eq} - T_\infty\right)}{\ln\left(\frac{R_o}{r_c}\right)\Delta\bar{H}_r} \tag{14}$$

$$\dot{m}_{NH_3} = M_{NH_3}\,\frac{2\pi L\lambda\left(T_{eq} - T_\infty\right)}{\Delta\bar{H}_r} \times \frac{1}{\ln\left(\frac{R_o}{r_c}\right)} \tag{15}$$

Equation (12) can be used to calculate the mass flow of ammonia at different times knowing the radius of the reaction zone. Considering Eq. (8), the mass flow of ammonia can be written as:

$$\dot{m}_{NH_3} = M_{NH_3}\,\frac{2\pi L\lambda\left(T_{eq} - T_\infty\right)}{\Delta\bar{H}_r} \times \frac{2}{\ln\left(\frac{1}{1 - X_{gs}}\right)} \tag{16}$$

### 2.2. Cooling through an internal tube

For the case of cooling from an internal tube placed along the cylinder axis, the solution follows in a manner similar to that developed for outside cooling. The rate of heat released from the moving reaction front is directly proportional to the net heat transfer.

An approximate analytical solution for cases with an internal cooling tube can also be obtained. It is assumed that the reaction is heat transfer limited and the pressure of the gas throughout the reactor is constant at $P = P_{sup}$. The reaction zone is assumed to be infinitesimally small and the heat transfer is assumed to be in the radial direction between the reaction zone and the cooling tube. The outer surface of the reactor is assumed to be insulated, and thus adiabatic boundary. Internal cooling:

$$\frac{(T-T_s)}{(T_{eq}-T_s)} = \frac{\ln(r/R_t)}{\ln(r_c/R_t)} \quad \text{for } R_t < r < r_c \tag{17}$$

And for internal heating:

$$\frac{(T-T_{eq})}{(T_s-T_{eq})} = 1 - \frac{\ln(r/R_t)}{\ln(r_c/R_t)} \tag{18}$$

$$q' = \frac{2\pi L\lambda(T_{eq}-T_s)}{\ln(r_c/R_t)} \tag{19}$$

The heat flux to the reaction front is proportional to its velocity:

$$4 \times \bar{\rho}_{salt}\Delta\bar{H}_r \times 2\pi r_c L \times \frac{dr_c}{dt} = \frac{2\pi\lambda L}{\ln\frac{r_c}{R_t}}\left(T_{eq} - T_\infty\right) \tag{20}$$

In Eqs. (17) to (20) $r_c$ is the radius of the reaction zone ($R_t < r_c < R_o$), and $R_t$ is the radius of the cooling tube. Rearranging Eq. (20), dividing both sides by $1/R_o^2$, integrating from $R_t$ to $r_c$, and applying the initial condition of $r_c = R_t$ at $t = 0$ gives:

$$\frac{1}{4}\left[\left(\frac{r_c}{R_t}\right)^2 \ln\left(\frac{r_c}{R_t}\right)^2 + 1 - \left(\frac{r_c}{R_t}\right)^2\right] = \frac{\lambda t}{4\times\bar{\rho}_{salt}\frac{\Delta\bar{H}_r}{(T_{eq}-T_\infty)}}\frac{1}{R_t^2} \tag{21}$$

$$\frac{1}{4}\left[\ln\left(\frac{R_o}{R_t}\frac{r_c}{R_o}\right)^2\left(\frac{r_c}{R_o}\right)^2 + \left(\frac{R_t}{R_o}\right)^2 - \left(\frac{r_c}{R_o}\right)^2\right] = \mathrm{Fo}_R \tag{22}$$

The relation between the scaled reaction progress and the radii of the reaction zone and reactor can be written as:

$$X_{gs} = \frac{X_g-0.2}{0.8} = \frac{r_c^2-R_t^2}{R_o^2-R_t^2} = \frac{\left(\frac{r_c}{R_o}\right)^2-\left(\frac{r_t}{R_o}\right)^2}{1-\left(\frac{R_t}{R_o}\right)^2} = \frac{\left(\frac{r_c}{R_o}\right)^2-R_r^2}{1-R_r^2} \tag{23}$$

In Eq. (23), $R_r$ is simply defined as the ratio of the radius of the cooling tube to the radius of the reactor tube ($R_r = R_t/R_o$). Therefore:

$$\left(\frac{r_c}{R_o}\right)^2 = X_{gs}(1-R_r^2) + R_r^2 \tag{24}$$

Equation (22) becomes:

$$\frac{1}{4}\left[\ln\left(X_{gs}\left(\frac{1}{R_r^2}-1\right)+1\right)\left(X_{gs}(1-R_r^2)+R_r^2\right)-\ X_{gs}(1-R_r^2)\right]=\ Fo_R \tag{25}$$

Although Eq. (25) has a more complex form than Eq. (22), the left-hand side of the equation is written as a function of the scaled reaction progress ($X_{gs}$) and the ratio of the cooling tube and the reactor tube radii such that the upper bound for Fourier number, defined by Eq. (11), can be obtained by setting $X_{gs}=1$:

$$\frac{1}{4}\left[\ln\left(\frac{1}{R_r^2}\right)-(1-R_r^2)\right]=Fo_R|_{X_g=1}=\frac{\lambda}{\frac{\Delta H_r}{(T_{eq}-T_\infty)}\times 4\bar{\rho}_{salt}}\frac{1}{R_o^2}t_{X_g=1} \tag{26}$$

Equation (26) estimates the duration of the absorption process in reactors with an internal cooling tube of radius $R_t$ and reactor radius of $R_o$.

Similar to the relationship specified for heating from at $R_o$, the mass flow rate of ammonia for reactors with internal cooling tubes can be calculated at different times knowing the radius of the reaction zone from:

$$\dot{m}_{NH_3}=M_{NH_3}\ \frac{2\pi L\lambda(T_{eq}-T_\infty)}{\Delta\bar{H}_r}\times\frac{1}{\ln\left(\frac{r_c}{R_t}\right)} \tag{27}$$

By rearranging Eq. (19) and calculating $r_c/R_t$, Eq. (20) can be written as:

$$\dot{m}_{NH_3}=M_{NH_3}\ \frac{2\pi L\lambda(T_{eq}-T_\infty)}{\Delta\bar{H}_r}\times\frac{2}{\ln\left(\frac{X_{gs}}{R_r^2}-X_{gs}+1\right)} \tag{28}$$

## 3. Results

The theoretical model's prediction of the absorption curves (global reaction progress) and mass flow rates are compared to simulations for both external and internal cooling. The mass flow rates predicted by the models are also compared to simulated values at a few different times and geometries in the following sections.

### 3.1. External Cooling

The predictions of the theoretical model of the extent of reaction scaled with the reaction Fourier number (Eq. (12)) are compared to seven different simulations of cooling from the outside surface in Figure 4 As is seen in this figure, the simple model reasonably captures the dominant heat transfer processes, both the overall rate of adsorption (time derivative of the extent of reaction) and a conservative time estimate for completion of the reaction as predicted by Eq. (12) ($Fo_{R,T}$ *=1/4*).

Mass fluxes predicted by Eq. (15) can also be compared with simulations for a specific geometry at specific times. Figure 5 compares the simulated mass fluxes and those obtained from the analytical model. The simulation models and comparison with the experiments are discussed in [1], [2]. Again, good agreement is found between the simulated mass fluxes and results of the simplified model, verifying the applicability of analytical models that track the reaction front through energy balances. Figure 5 shows that for the smaller reactor with the outer radius of 25mm, the numerical model has a better agreement with the analytical model than the larger reactor with outer radius of 125 mm. It is of note that in the numerical models the reactor has the length of L=200mm. Therefore, the cooling effect of the end surfaces of the reactor increase the absorption rate. This effect is larger in the larger reactor ($R_o$ = 125mm), increasing the mass flow rate of the gas, and deviating from the numerical model.

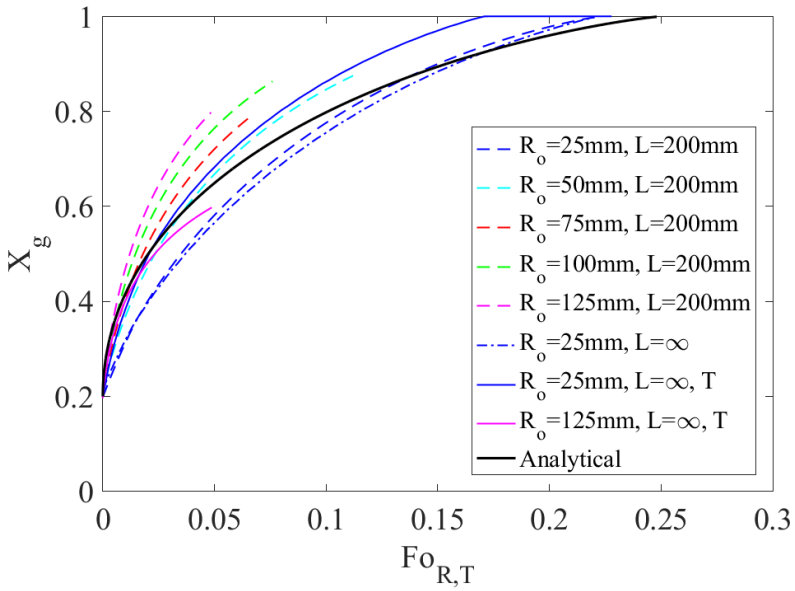


Figure 4 - Absorption curves for outside cooling with normalized times.

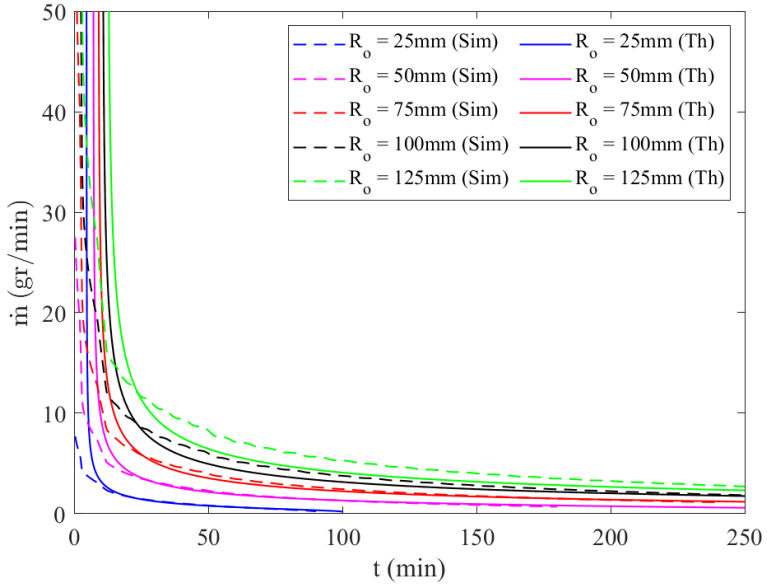


Figure 5 - Comparison of simulations with predicted mass flow rates of gas for cases with outside and radii ranging from 25mm to 125mm.

### 3.2. Cooling from Inner Tube

A comparison of the approximate analytical solution to the numerical simulation for various values of $R_t$ and constant tube to reactor radii ratios ($R_t/R_o$), replotted according to the dimensionless Fourier number, is shown in Figure 6. As shown, the absorption behaviours of all cases are similar when normalized. Further, the analytical model well represents the general behaviour of all simulations and specific behaviour of those simulations most closely matching the conditions of the model assumptions. It is worth mentioning that the larger reactors require longer absorption processes and the simulation time becomes too long. All reactors are simulated with equal durations, and when the absorption curves are normalized with respect to time, the reaction Fourier number becomes smaller and the length of the curves shown in Figure 6 becomes shorter.

Figure 7 shows the mass flow rate of ammonia per unit length of the reactor for cases with a similar internal cooling tube. As Figure 7 shows, the absorption rate of ammonia settles to an asymptote value over time. This figure also shows that the absorption rate for reactors with an internal cooling tube mainly depend on the radius of the tube. Therefore, relatively constant mass flow rates of ammonia gas can be produced by utilizing reactors with internal cooling tubes with high convective heat transfer coefficients.

During the absorption in a reactor cooled through an internal tube, both the thermal resistance between the reaction zone (at $r_c$) and the cooling surface, and the area of the reaction zone increase. One can argue that these two effects balance each other and the reaction rate stays relatively constant.

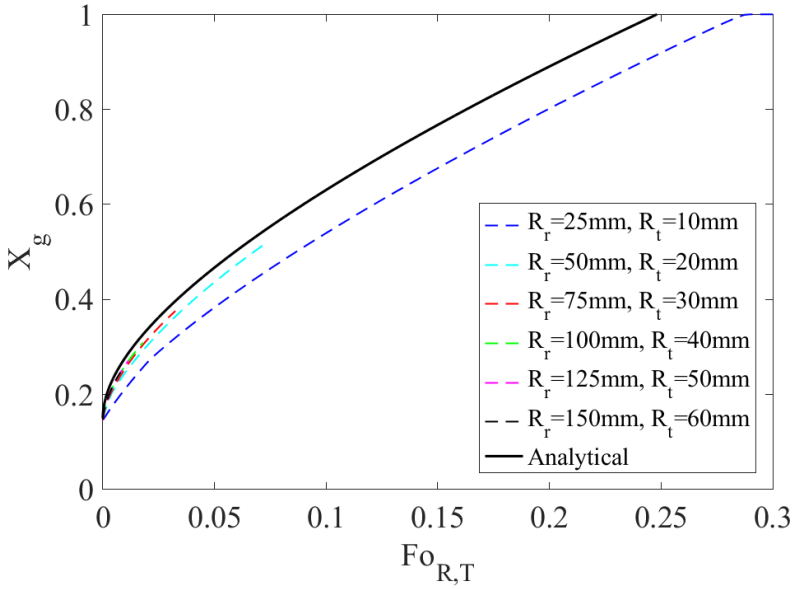


Figure 6 - The normalized absorption curves for reactors with internal cooling and identical reactor to cooling tube radius ratios.

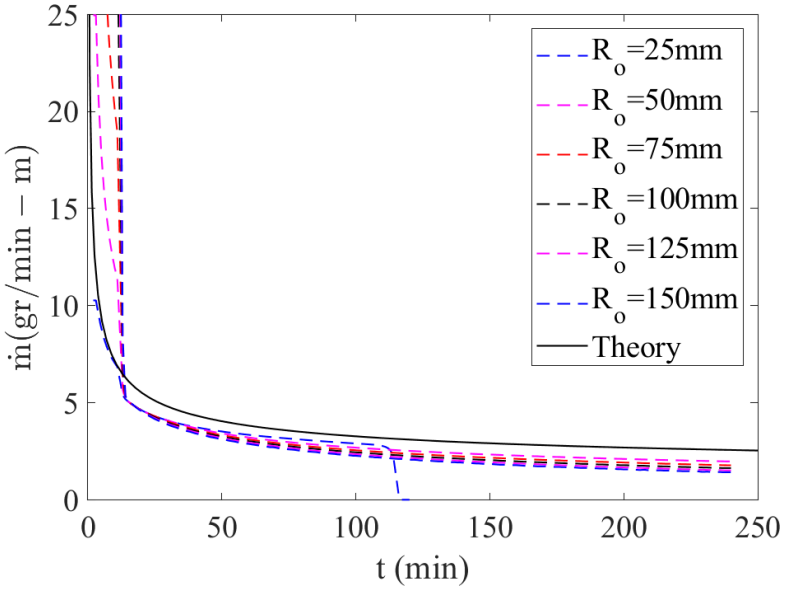


Figure 7 - Mass flow rate of cases with an internal cooling tube of radius $R_t$=10mm, compared with the analytical solution.

## 4. Discussion

The simple models that describe of the dominant processes controlling the performance of cylindrical thermochemical reactive matrices, with the heat transfer surface either located on the exterior wall or a tube carrying heat transfer fluid located along the cylinder axis, have been shown to apply to the simulated cases for cooling a matrix comprised of $MgCl_2.2NH_3$, subjected to a specified ammonia gas pressure and boundary temperature. Through generalization and mathematical extrapolation, the theory was found to apply to the heating mode as well.

One difference exists between the heating and cooling modes, however. The thermal conductivity of the matrix, and its value ($\lambda$) used in defining the reaction Fourier number would be different for heating versus cooling. For the cooling case, heat is being transferred from the reaction front though fully saturated absorbent with a higher thermal conductivity than the case of heating, where the heat is being transferred through desaturated absorbent with a lower thermal conductivity. Those different thermal conductivities should be assigned appropriately to determine actual times from the reaction Fourier number for heating or cooling time estimates.

## 5. Conclusion

Analytical models were developed for the adsorption and desorption processes during the recharge and operational modes of a cylindrical thermochemical battery, heated or cooled from the external boundary or an internal cooling tube. The models were shown to represent the dominant processes observed in the absorption simulations presented before [1]. The models allow for the generalization of the simulation results to other absorbent/gas pairs [3], [11]–[15], and application to both operational and charging modes. It was found that for external heating or cooling from a surface at constant temperature, the reaction should near completion at a reaction Fourier number of 0.25 - 0.30. For internal heating, that value depends on the ratio of the outer to inner tube radii, and can be explicitly defined through that ratio. Thus, these models can be used to effectively design cylindrical thermochemical batteries or solid-state ammonia storage systems to meet specific heat transfer rates, gas absorption or release rates, operational temperatures, and energy storage capacities without the need for complex simulation packages.

## Acknowledgements

We would like to thank Advanced Research Projects Agency-Energy (ARPA-E, DE-AR0000173) and Department of Mechanical Engineering at The University of Utah for funding this project.

## References

[1] S. A. Hedayat Mofidi, "Analysis and Parametric Study of Magnesium Chloride and Ammonia Thermochemical Energy Storage Systems and Thermal Batteries," PhD. Dissertation, University of Utah, Salt Lake City, Utah, 2019.

[2] S. A. Hedayat Mofidi and K. S. Udell, "Study of Heat and Mass Transfer in MgCl2/NH3 Thermochemical Batteries," *J. Energy Resour. Technol.*, vol. 139, no. 3, pp. 032005-032005–10, Feb. 2017, doi: 10.1115/1.4035750.

[3] P. Neveu and J. Castaing, "Solid-gas chemical heat pumps: Field of application and performance of the internal heat of reaction recovery process," *Heat Recovery Syst. CHP*, vol. 13, no. 3, pp. 233–251, May 1993, doi: 10.1016/0890-4332(93)90014-M.

[4] I. Dincer and M. Rosen, *Thermal Energy Storage: Systems and Applications*. Chichester, W. Sussex, UK: John Wiley & Sons, 2002.

[5] C.-J. Winter, R. L. Sizmann, and L. L. Vant-Hull, *Solar Power Plants: Fundamentals, Technology, Systems, Economics*. Berlin: Springer Science & Business Media, 2012.

[6] K. S. Udell, B. Kekelia, P. Fan, C. Zhou, and Z. Fang, "Performance of a Multi-Cell MgCl2/NH3 Thermo-Chemical Battery During Recharge and Operation," in *Proceedings of the ASME 2015 Power and Energy Conversion Conference*, San-Diego, Jun. 2015, p. V001T03A004-9. doi: 10.1115/ES2015-49508.

[7] Z. Z. Fang, C. Zhou, P. Fan, K. S. Udell, R. C. Bowman, J. J. Vajo, J. J. Purewal, B. Kekelia, "Metal hydrides based high energy density thermal battery," *J. Alloys Compd.*, vol. 645, Supplement 1, pp. S184–S189, Oct. 2015, doi: 10.1016/j.jallcom.2014.12.260.

[8] S. A. H. Mofidi and K. S. Udell, "Permeability of MgCl2- Graphite Reactive Compound," *Res. Dev. Mater. Sci.*, vol. 14, no. 4, pp. 1572–1576, Dec. 2020.

[9] J. H. Han, K.-H. Lee, D. H. Kim, and H. Kim, "Transformation Analysis of Thermochemical Reactor Based on Thermophysical Properties of Graphite−MnCl2 Complex," *Ind. Eng. Chem. Res.*, vol. 39, no. 11, pp. 4127–4139, Nov. 2000, doi: 10.1021/ie9904394.

[10] N. Mazet, M. Amouroux, and B. Spinner, "Analysis and Experimental Study of the Transformation of a Non-Isothermal Solid/Gas Reacting Medium," *Chem. Eng. Commun.*, vol. 99, no. 1, pp. 155–174, 1991, doi: 10.1080/00986449108911585.

[11] H.-B. Lu, N. Mazet, and B. Spinner, "Modelling of gas-solid reaction—Coupling of heat and mass transfer with chemical reaction," *Chem. Eng. Sci.*, vol. 51, no. 15, pp. 3829–3845, Aug. 1996, doi: 10.1016/0009-2509(96)00010-3.

[12] R. Iwata, T. Yamauchi, Y. Hirota, M. Aoki, and T. Shimazu, "Reaction kinetics of ammonia absorption/desorption of metal salts," *Appl. Therm. Eng.*, vol. 72, no. 2, pp. 244–249, Nov. 2014, doi: 10.1016/j.applthermaleng.2014.07.034.

[13] J. Li, "Isothermal hydrogenation kinetics of magnesium-based hydride," Ph.D. Thesis, University of Utah, Salt Lake City, Utah, 2014.

[14] V. Goetz and A. Marty, "A model for reversible solid-gas reactions submitted to temperature and pressure constraints: simulation of the rate of reaction in solid-gas reactor used as chemical heat pump," *Chem. Eng. Sci.*, vol. 47, no. 17–18, pp. 4445–4454, Dec. 1992, doi: 10.1016/0009-2509(92)85122-R.

[15] A. H. Abedin and M. A. Rosen, "A Critical Review of Thermochemical Energy Storage Systems," *Open Renew. Energy J.*, vol. 4, no. 1, pp. 42–46, Aug. 2011.